Liproxstatin-1 induces cell cycle arrest, apoptosis, and caspase-3/GSDME-dependent secondary pyroptosis in K562 cells

HAI-QUN DONG*, SHI-JING LIANG*, YU-LING XU, YI DAI, NA SUN, DONG-HONG DENG and PENG CHENG

Department of Hematology, The First Affiliated Hospital of Guangxi Medical University, Nanning,
Guangxi Zhuang Autonomous Region 530021, P.R. China

Abstract. Leukemia is a fatal hematopoietic disorder with a poor prognosis. Drug resistance is inevitable after the long-term use of chemotherapeutic agents. Liproxstatin-1, commonly known as a ferroptosis inhibitor, has never been reported to have anticancer effects. In the present study, the antileukemic role of liproxstatin-1 in K562 leukemia cells was investigated. Liproxstatin-1 inhibited K562 cell proliferation in a dose- and time-dependent manner. RNA sequencing revealed several pathways that were affected by liproxstatin-1, such as the G1/S transition of the mitotic cell cycle and extrinsic or intrinsic apoptotic signaling pathways. The results of flow cytometry indicated that liproxstatin-1 arrests the cell cycle at the G1 phase, and even at the G2/M phase. $p21^{WAF1/CIP1}$, a cyclin-dependent kinase inhibitor, was upregulated. It was also determined that liproxstatin-1 induced BAX and TNF-α expression, which was accompanied by cleavage of caspase-3 and PARP. The caspase-3-specific inhibitor z-DEVD-FMK rescued some of the apoptotic cells. Interestingly, K562 cells were characterized by swelling and plasma membrane rupture when treated with a high concentration of liproxstatin-1, which was inconsistent with the typical apoptotic appearance. Thus, it was hypothesized that apoptosis-mediated pyroptosis occurs during liproxstatin-1-induced cell death. The expression of the hallmark of pyroptosis, the cleaved N-terminal GSDME, increased. Additionally, it was observed that endoplasmic reticulum stress and autophagy were involved in liproxstatin-1-induced cell death. Collectively, liproxstatin-1 induced cell cycle arrest, apoptosis, and caspase-3/GSDME-dependent secondary pyroptosis in K562 leukemia cells, which provides new hope for the treatment of leukemia.

Introduction

Leukemia is a life-threatening hematopoietic malignancy characterized by the malignant proliferation of hematopoietic stem cells and dysregulation of regulated cell death (RCD) (1-3). The age-standardized 5-year relative survival rate of Chinese patients with leukemia increased from 19.6% in 2003-2005 to 25.4% in 2012-2015 owing to progression in pathogenesis and therapeutic strategies for leukemia (4). However, side effects and drug resistance are inevitable after the long-term use of chemotherapeutic drugs (5). Thus, new antileukemic drugs need to be discovered.

A delicate balance between RCD and cell proliferation is essential to maintain a healthy cell population; however, this balance is out of control in leukemia cell populations. Conventional drugs, such as cytarabine and daunorubicin, are used to treat leukemia via the induction of DNA damage and cell cycle arrest (6). The novel oral drug venetoclax, which targets the apoptotic pathway, has been approved by the Food and Drug Administration for acute myeloid leukemia (7,8).

Pyroptosis is a novel form of RCD characterized by cell swelling, plasma membrane rupture, and DNA condensation and fragmentation (9,10). Gasdermins play a pivotal role in pyroptosis. Apart from APJK (DFNB59), all gasdermins (GSDMA-E) share the gasdermin N-terminal effector domain (11-13). The N-terminal effector domain is activated by the caspase-dependent cleavage of GSDMD or GSDME and exhibits pore-forming, intrinsic cytotoxic, and antibacterial properties (11,12). Activated caspase-1 and caspase-4/5/11 are responsible for canonical and non-canonical GSDMD-related pyroptosis, respectively (14,15). Activated caspase-3 that is induced by tumor necrosis factor (TNF)-α or DNA-damaging chemotherapeutic drugs are responsible for GSDME-related pyroptosis (10,13,16). Preclinical studies involving GSDMD-related pyroptosis induced by DPP8/9 inhibitors and GSDME-related pyroptosis induced by pyridoxine, aimed at the treatment of acute myeloid leukemia, have indicated that pyroptosis is a new target for the management of leukemia (17-19). Apoptosis, characterized by cytoplasmic shrinkage and small apoptotic bodies, also commonly known as type I cell death, is a classical form of RCD mediated by

---

Correspondence to: Professor Peng Cheng, Department of Hematology, The First Affiliated Hospital of Guangxi Medical University, 6 Shuangyong Road, Nanning, Guangxi Zhuang Autonomous Region 530021, P.R. China
E-mail: gxchengpeng@163.com

*Contributed equally

the activation of caspase-3 (10). As caspase-3 is activated in both pyroptosis and apoptosis, the final cell destination is dependent on the expression levels of GSDME (20). It is generally accepted that GSDME-positive cells undergo pyroptosis, whereas GSDME-negative cells develop apoptotic responses (13,16). Autophagy, commonly known as type II cell death, is a core molecular process that maintains cellular and organismal homeostasis (21). Notably, increasing evidence suggests the existence of multilevel crosstalk between different types of RCD (20,22-24).

Liproxstatin-1 (Lip-1) is a small molecule with a variety of biological properties, including antibacterial and anti-ferroptosis activities (25,26). However, the antileukemic effect of Lip-1 has not yet been reported. The leukemia cell line K562, derived from a patient with chronic myeloid leukemia during the blast crisis in the 1970s (27), is a good cellular model for *in vitro* research. K562 cells express low levels of GSDME (13), suggesting that K562 cells will develop apoptotic responses prior to secondary necrotic responses following treatment with certain chemotherapeutic drugs and cleavage of caspase-3. Interestingly, Lip-1-treated K562 cells developed caspase-3/GSDME-dependent secondary pyroptosis after apoptosis. Moreover, the results indicated that endoplasmic reticulum (ER) stress, autophagy, and cell cycle arrest were involved in the modulation of K562 cell proliferation. Taken together, Lip-1 may provide new hope for the treatment of leukemia.

Materials and methods

Antibodies and reagents. Lip-1 (cat. no. S7699) was purchased from Selleck Chemicals. Z-DEVD-FMK (cat. no. HY-12466) was purchased from MedChemExpress. RPMI-1640 medium (cat. no. 11835-030) was purchased from Thermo Fisher Scientific, Inc., fetal bovine serum (cat. no. 900-108) was purchased from Gemini Bio Products, and penicillin-streptomycin (product no. V900929) was purchased from Sigma-Aldrich; Merck KGaA. CryoStor CS10 (cat. no. 07930) was obtained from StemCell Technologies, Inc. Dimethyl sulfoxide and Dulbecco's phosphate-buffered saline (PBS) were purchased from Dalian MeilunBio Biotechnology Co., Ltd. QuickBlock Blocking Buffer for western blotting was purchased from Beyotime Institute of Biotechnology. Thermo Scientific PageRular Prestained Protein Ladder (cat. no. 26616) was purchased from Thermo Fisher Scientific, Inc. SH-SY5Y whole cell lysate used as the positive control for GSDME-N-terminal in western blotting was gifted by Abcam.

The primary antibodies used were as follows: C/EBP homologous (CHOP) antibody (cat. no. 15204-1-AP) and PUMA antibody (cat. no. 55120-1-AP) obtained from ProteinTech Group, Inc.; LC3A/B (D3U4C) antibody (product no. 12741) and cleaved caspase-3 (ASP175) antibody (product no. 9661) purchased from Cell Signaling Technology, Inc.; CDKN1A/p21CIP1 antibody (cat. no. A19094) obtained from ABclonal Biotech Co., Ltd.; anti-DFNA5/GSDME-N-terminal antibody (product code ab215191) obtained from Abcam; GSDME antibody-N-terminal (cat. no. AF4016) from Affinity Biosciences, Ltd.; and β-tubulin antibody (cat. no. M30109), BCL2 associated X (BAX) antibody (product no. T40051), caspase-3 antibody (product no. T40044), PARP antibody (product no. T40050), and actin (2P2) antibody (product no. M20011) were gifted by Abmart Pharmaceutical Technology Co., Ltd. The β-tubulin antibody served as a loading control. The secondary antibody, goat anti-rabbit mouse IgG-HRP (product no. M21003) was gifted by Abmart. Cy3-conjugated goat anti-mouse IgG (H+L) (product no. GB21301) and FITC-conjugated goat anti-rabbit IgG (H+L) (product no. GB22303) were purchased from Wuhan Servicebio Technology Co., Ltd.

Cell culture. The K562 cell line (human leukemia cell line) (cat. no. CL-0130) and SH-SY5Y cell line (cat. no. CL-0208) were purchased from Procell Life Science & Technology Co., Ltd. K562 and SH-SY5Y cells were cultured in RPMI-1640 medium containing 10% (v/v) fetal bovine serum, penicillin (100 U/ml), and streptomycin (100 μg/ml). Cells were grown at 37˚C in a 5% CO_2 incubator. The K562 cell line tested mycoplasma-negative using a GMyc-PCR Mycoplasma Test Kit (Shanghai Yeasen Biotechnology, Inc.), according to the manufacturer's instructions. Cell identities of K562 and SH-SY5Y cell lines were authenticated by Genetic Testing Biotechnology Corp. using short tandem repeat profiling.

Cell viability assay. Exponentially growing K562 cells were seeded at a density of $1x10^4$ cells/well in 100 μl of RPMI-1640 medium in 96-well plates. Lip-1 was dissolved in dimethyl sulfoxide, and cells were treated with various concentrations (2, 4, 10, 20, or 40 μM) of Lip-1 for 24 or 48 h. Subsequently, 10 μl of CCK-8 solution (Dalian MeilunBio Biotechnology Co., Ltd.) was added to each well, and the 96-well plate was incubated at 37˚C for 3 h in the dark. The absorbance (A) was measured at 450 nm using a Varioskan LUX microplate reader (Life Technologies; Thermo Fisher Scientific, Inc.). Cell viability was calculated using the following formula: Viability (%)=[(A$_{drug}$-A$_{blank}$)/(A$_{control}$-A$_{blank}$)] x100%. The half-maximal inhibitory concentration was calculated using GraphPad Prism 7 (GraphPad Software, Inc.). In other experiments, K562 cells were pretreated with the caspase-3-specific inhibitor z-DEVD-FMK at a concentration of 200 μM for 3 h, and further treated with 20 μM Lip-1 for 12 h. The CCK-8 assay was performed to determine cell viability.

Microscopy. To investigate the morphology of apoptotic cells, K562 cells were seeded in a 6-well plate ($2x10^5$ cells/ml) and subjected to Lip-1 treatment at a concentration of 10 or 20 μM for 24 h. Dimethyl sulfoxide at a dilution of 5/10,000 served as the vehicle control. Static bright-field images were captured using an IX71 microscope (Olympus Corporation).

Scanning electron microscopy. To further investigate the morphological changes in Lip-1-induced K562 cells, scanning electron microscopy was performed on K562 cells seeded in 6-well plates ($2x10^5$ cells/ml) and treated with 10 or 20 μM Lip-1 for 24 h. The cells were then washed with PBS, double-fixed in 2.5% glutaraldehyde and 1% osmic acid at room temperature for 2 h, dehydrated using ethanol solutions, and dried with a critical point dryer. Finally, the specimens were coated with gold using carbon stickers for 30 sec and visualized under a Hitachi SU8100 scanning electron microscope (Hitachi, Ltd.).

Transmission electron microscopy. To examine the ultrastructural damage in Lip-1-induced K562 cells, transmission electron microscopy was performed on K562 cells, and the cells at a density of $2x10^5$ cells/ml were treated with 10 or 20 μM Lip-1. The cells were then washed with PBS, double-fixed in 2.5% glutaraldehyde and 1% osmic acid at room temperature for 2 h, dehydrated using a series of ethanol solutions, and embedded at 60°C for 48 h in SPI-PON 812 resin (SPI; Structure Probe, Inc.). Finally, after polymerization, ultrathin sectioning (resin blocks were cut to 60-80 nm thickness using an ultramicrotome), and staining procedures (2% uranium acetate saturated alcohol solution staining in the dark for 8 min, 2.6% lead citrate staining for 9 min) the cuprum grids were placed into the grid board and dried at room temperature overnight. The specimens were visualized using a Hitachi HT7800 transmission electron microscope (Hitachi, Ltd.).

DNA fragmentation evaluation. K562 cells at a density of $2x10^5$ cells/ml were cultured in a 6-well plate, followed by treatment with 10 or 20 μM Lip-1 for 24 h. K562 cells were fixed in 4% paraformaldehyde at room temperature for 2 h. DNA fragmentation evaluation assay was performed using the FITC TUNEL Cell Apoptosis Detection Kit (Wuhan Servicebio Technology Co, Ltd.), according to the manufacturer's instructions, and the specimens were stained with DAPI at room temperature avoiding light for 10 min. For the positive control, samples were treated with 2 U/ml DNase I (Wuhan Servicebio Technology Co, Ltd.) for 10 min. Whole-mounted specimens were imaged using a fluorescence microscope (Nikon Corporation). DNA fragmentation was measured as follows: Four randomly selected fields per section, equivalent to at least 600 cells, were manually analyzed using ImageJ software V 1.8.0 (National Institutes of Health).

Immunofluorescence and confocal microscopy. To study the effect of Lip-1 on autophagosome formation, an immunofluorescence assay was performed on K562 cells seeded in 6-well plates and treated with 10 or 20 μM Lip-1 for 24 h. Following treatment, the cells were fixed with 4% paraformaldehyde at room temperature for 2 h, permeabilized with 0.1% Triton X-100 (Sigma-Aldrich: Merck KGaA), blocked with 3% bovine serum albumin at room temperature for 30 min, and incubated with primary antibodies (LC3A/B and actin) at a dilution of 1:300 overnight at 4°C. Next, the cells were incubated with Cy3-conjugated goat anti-mouse IgG (H+L) and FITC-conjugated goat anti-rabbit IgG (H+L) at a dilution of 1:500 at room temperature avoiding light for 50 min, and the nuclei were counterstained with DAPI at room temperature avoiding light for 10 min. Specimens were visualized using a confocal laser-scanning microscope (Nikon Corporation). The ratio of LC3-positive cells was measured as follows: Two randomly selected fields per section, equivalent to at least 100 cells, were manually analyzed using ImageJ software V 1.8.0.

RNA sequencing and differential expression analysis. K562 cells were treated with 10 or 20 μM Lip-1 for 24 h. Total RNA was isolated using TRIzol reagent (Invitrogen; Thermo Fisher Scientific, Inc.), and then sent to Genesky Bio-Tech Co., Ltd. for RNA sequencing (RNA-seq) and differential expression analysis. Briefly, libraries were constructed using the TruSeq RNA Sample Preparation Kit v2 (Illumina, Inc.) and purified using the Agencourt SPRIselect Reagent Kit (Beckman Coulter, Inc.). Sequencing data were analyzed using StringTie (28), to determine the expression level of each gene. Following DESeq2 (29), genes with $|\log_2(\text{fold-change})| >1$ and adjusted P<0.05 were regarded as differentially expressed genes (DEGs). Volcano plots were constructed based on DEGs. Gene Ontology (30) and Kyoto Encyclopedia of Genes and Genomes (31) analyses were performed to assess gene enrichment and functional annotation using clusterProfiler (32). Raw sequencing data were submitted to GEO (GSE205036).

Reverse transcription-quantitative polymerase chain reaction (RT-qPCR). Total RNA was isolated from K562 cells using TRIzol reagent, and complementary DNA was produced using the PrimeScript RT Reagent Kit (Takara Bio, Inc.), according to the manufacturer's instructions. RT-qPCR was conducted on an Applied Biosystems 7500 Real-Time PCR System (Applied Biosystems; Thermo Fisher Scientific, Inc.) using TB Green Premix Ex Taq II (Takara Bio, Inc.). Relative gene expression was calculated using the $2^{-\Delta\Delta Cq}$ method (33) and normalized to that of RPLP0. Human RPLP0 endogenous reference gene primers were obtained from Sangon Biotech Co., Ltd. The sequences of the primers used for RT-qPCR were as follows: RPLP0 forward, 5'-GCAGCATCTACAACCCTGAAG-3' and reverse, 5'-CACTGGCAACATTGCGGAC-3'; DDIT3 forward, 5'-GGAAACAGAGTGGTCATTCCC-3' and reverse, 5'-CTGCTTGAGCCGTTCATTCTC-3'; BBC3 forward, 5'-GACCTCAACGCACAGTACGAG-3' and reverse, 5'-AGGAGTCCCATGATGAGATTGT-3'; MAP1LC3B forward, 5'-GAGAAGACCTTCAAGCAGCG-3' and reverse, 5'-TATCACCGGGATTTTGGTTG-3'; CDKN1A forward, 5'-TGTCCGTCAGAACCCATGC-3' and reverse, 5'-AAAGTCGAAGTTCCATCGCTC-3'; TNF forward, 5'-GAGGCCAAGCCCTGGTATG-3' and reverse, 5'-CGGGCCGATTGATCTCAGC-3'; and GSDME forward, 5'-TGCCTACGGTGTCATTGAGTT-3' and reverse, 5'-TCTGGCATGTCTATGAATGCAAA-3'.

Cell cycle assay. Cell cycle analysis was conducted using a Cell Cycle Staining Kit [Hangzhou Multi Sciences (Lianke) Biotech Co., Ltd.], according to the manufacturer's instructions. Briefly, K562 cells treated with or without Lip-1 were harvested, washed twice with PBS, and treated with 1 ml DNA staining solution and 10 μl permeabilization solution at 4°C in the dark for 30 min. Finally, single-cell suspensions were analyzed using a BD FACSCalibur flow cytometer (BD Biosciences). Data were analyzed using FlowJo software v10.0.8 (BD Biosciences).

Annexin V-FITC/PI double staining assay. The integrity of the cell membrane was evaluated using an Annexin V-FITC/PI Apoptosis Kit [Hangzhou Multi Sciences (Lianke) Biotech Co., Ltd.], according to the manufacturer's instructions. Briefly, K562 cells treated with 10 or 20 μM Lip-1 for 24 h were harvested, washed twice with binding buffer, and stained with Annexin V-FITC and PI at 4°C in the dark for 10 min. Finally, the cells were analyzed using a BD FACSCalibur flow

cytometer, and the data were analyzed using FlowJo software v10.0.8.

Western blotting. Total protein was extracted from the cells using RIPA lysis buffer (Dalian MeilunBio Biotechnology Co., Ltd.). After measuring the protein concentration using a BCA Protein Assay Kit (Beyotime Institute of Biotechnology), 15 μg of total protein was loaded onto 12.5% sodium dodecyl sulfate-polyacrylamide gel electrophoresis gels, processed for electrophoresis, transferred to a polyvinylidene fluoride membrane (Merck KGaA). The polyvinylidene fluoride membranes were blocked with QuickBlock™ Blocking Buffer (cat. no. P0252; Beyotime Institute of Biotechnology) at room temperature for 15 min. Membranes were incubated with C/EBP homologous (CHOP) antibody (1:1,000 dilution), PUMA antibody (1:1,000 dilution), LC3A/B (D3U4C) antibody (1:1,000 dilution), cleaved caspase-3 (ASP175) antibody (1:1,000 dilution), CDKN1A/p21CIP1 antibody (1:1,000 dilution), anti-DFNA5/GSDME-N-terminal antibody (1:1,000 dilution), GSDME antibody-N-terminal (1:1,000 dilution), β-tubulin antibody (1:8,000 dilution), BCL2 associated X (BAX) antibody (1:1,000 dilution), caspase-3 antibody (1:1,000 dilution) and PARP antibody (1:1,000 dilution) at 4°C for 12 h. Next, the membranes were incubated with goat anti-rabbit mouse IgG-HRP secondary antibody at room temperature for 1 h. The membranes were treated with Meilunbio® FGSuper Sensitive ECL Luminescence Reagent (cat. no. MA0186; Dalian MeilunBio Biotechnology Co., Ltd.), according to the manufacturer's instructions, and protein bands were scanned using GelDoc XR (Image Lab; Bio-Rad Laboratories, Inc.). Densitometric measurements of the protein bands were performed using ImageJ software v1.8.0.

Caspase-3 and caspase-1 activity assessment. Caspase-3 and caspase-1 activities were determined using Colorimetric Assay Kits (Dalian MeilunBio Biotechnology Co., Ltd.), which utilized two types of substrates: Ac-DEVD-pNA for caspase-3 and Ac-YVAD-pNA for caspase-1. Briefly, K562 cells at a density of $2x10^5$ cells/ml were cultured in 6-well plates, followed by treatment with 10 or 20 μM Lip-1 for 12 or 24 h. The cells were lysed in lysis buffer at 4°C for 15 min. Protein concentration was measured using a Bradford Assay Kit (Dalian MeilunBio Biotechnology Co., Ltd.). Following incubation, caspase-3 and caspase-1 activities were determined by measuring the changes in absorbance at 405 nm using a microplate reader.

Enzyme-linked immunosorbent assay (ELISA). K562 cells at a density of $1x10^6$ cells/ml were cultured in 6-well plates and treated with 10 or 20 μM Lip-1 for 24 h. Cell culture supernatants were collected, and cell lysates were harvested via centrifugation at 600 x g at 4°C for 5 min and lysed with lysis buffer at 4°C for 15 min. Protein concentration was determined using a Bradford Assay Kit. The levels of human TNF-α in the cell culture supernatants and cell lysates were detected using an ELISA Kit (cat. no. RK00030; ABclonal Biotech Co., Ltd.), according to the manufacturer's instructions. The relative TNF-α concentration in the cell lysates was calculated as follows: Relative TNF-α (pg/μg)=[(TNF-α concentration)/(protein concentration)]. The minimum detectable concentration was 6.9 pg/ml.

Statistical analysis. Quantitative variables are presented as the mean ± SD. SPSS 25.0 (IBM Corp.) was used for statistical analysis. Statistical analysis was performed using unpaired two-tailed Student's *t*-test for comparison of two groups and one-way ANOVA followed by Dunnett's post hoc test for comparison of three groups. The Benjamini-Hochberg adjusted P-value was used for sequencing data. P<0.05 was considered to indicate a statistically significant difference.

Results

Lip-1 inhibits viability of K562 leukemia cells in a dose-dependent and time-dependent manner. To verify ferroptosis induction in K562 leukemia cells by some agents, K562 cells were pre-treated with Lip-1 (an inhibitor of ferroptosis; Fig. 1A). In the Lip-1-treated group, cell death was observed under a microscope, and the result revealed that the viability of K562 cells decreased. The antileukemic effect of Lip-1 has yet to be reported. Thus, K562 cells were treated with a series of Lip-1 concentrations (0, 2, 4, 10, 20, and 40 μM) for different lengths of time (24 and 48 h) and K562 cell viability was assessed using the CCK-8 assay. The inhibitory effect of Lip-1 on cell viability was dose-dependent and time-dependent; the 24- and 48-h half-maximal inhibitory concentrations of Lip-1 in K562 cells were 11.4 and 8.1 μM, respectively (Fig. 1B). Based on CCK-8 assay data, K562 cells treated with 10 and 20 μM Lip-1 for 24 h were regarded as the experimental groups, and these groups were used for subsequent experiments.

Lip-1 induces ultrastructural changes in K562 cells. Because Lip-1-induced cell death remains largely unknown, the ultra-structural changes in K562 cells were examined. Excessive cell swelling was observed in Lip-1-treated K562 cells in phase-contrast images (Fig. 1C). With higher magnification via SEM, it was observed that untreated K562 cells had intact plasma membranes with abundant microvilli whereas 10 μM Lip-1-treated K562 cells had large membrane bubbles with breakage; furthermore, loss of microvilli and membrane pores of varying sizes were observed in K562 cells after 20 μM Lip-1 treatment (Fig. 1D). Additionally, TEM images depicted the rupture of the plasma membrane, an expanded rough endoplasmic reticulum (RER), and the increased number of autolysosomes (Fig. 2A-C).

RNA-seq of the effects of Lip-1 on K562 cells. To explore the molecular mechanisms underlying Lip-1-induced cell death, RNA-seq was performed on K562 cells treated with 0, 10, 20 μM Lip-1. To confirm the type of cell death, DEGs were annotated via GO analysis, and the main biological processes regulated by Lip-1, including G1/S transition of miotic cell cycle, the extrinsic apoptotic signaling pathway, and the intrinsic apoptotic signaling pathway (Fig. 3A and B) were identified. By analyzing sequencing data, DEGs were distin-guished and volcano plots were constructed (Fig. 3C and D). In addition, KEGG analysis indicated that signaling pathways that are fundamental for the modulation of cell proliferation and death, including autophagy and apoptosis, were deeply affected by Lip-1 treatment (Fig. 3E and F). Collectively, these results demonstrated that cell-cycle arrest, apoptosis,
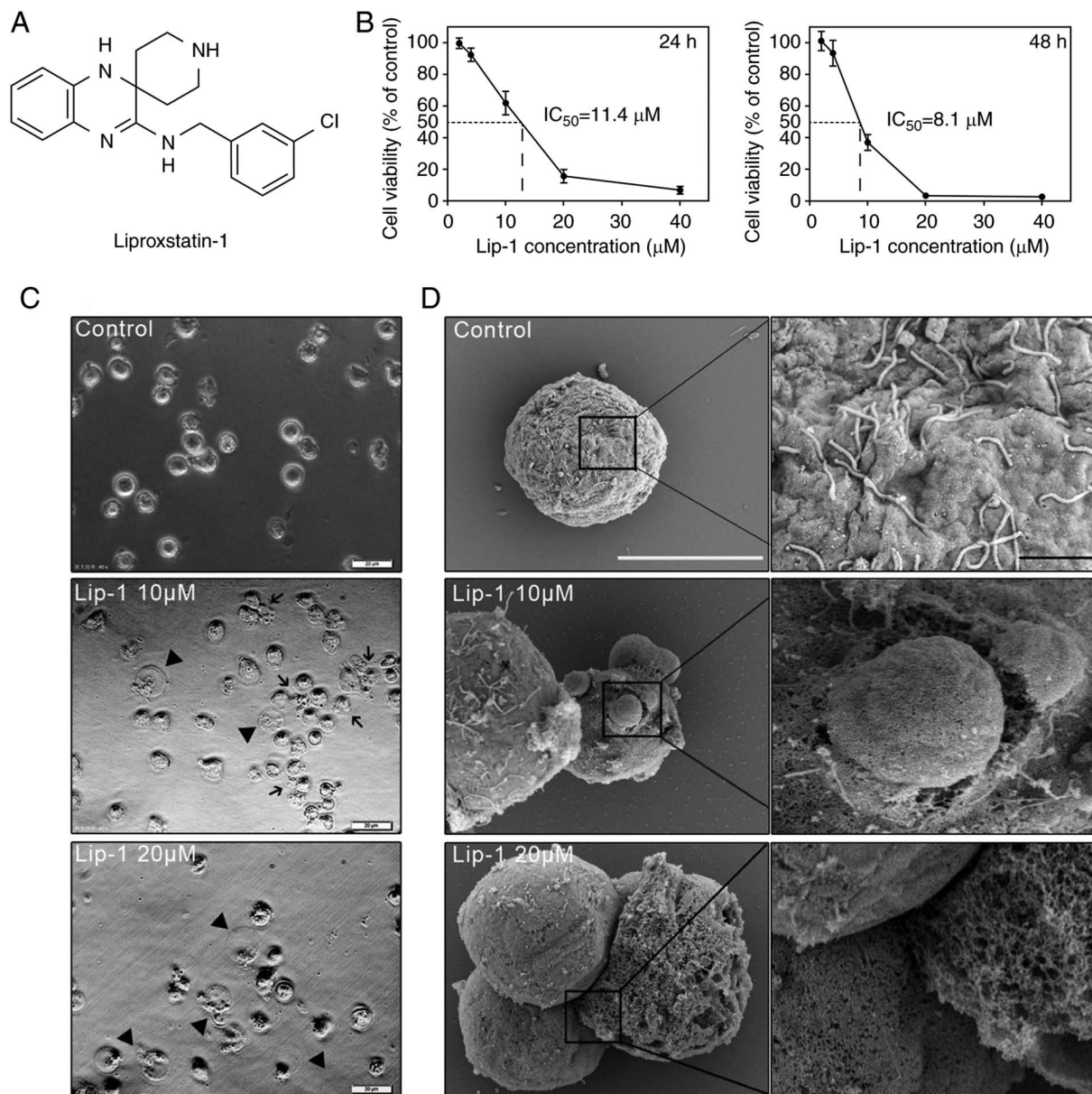
Figure 1. Viability and morphology of K562 cells treated with Lip-1. (A) Chemical structure of Lip-1. (B) Lip-1 inhibited the viability of K562 cells in a concentration- and time-dependent manner. Data are expressed as the mean ± SD (n=3). (C) Phase-contrast images of K562 cells treated with 10 and 20 μM Lip-1 for 24 h. Arrowheads indicate pyroptotic cells; arrows indicate apoptotic cells. Scale bar, 20 μm. (D) Morphological characteristics of K562 cells treated with Lip-1 for 24 h visualized via scanning electron microscopy. White scale bar, 10 μm; black scale bar, 1 μm. Lip-1, liproxstatin-1; IC$_{50}$, half-maximal inhibitory concentration.

and autophagy are involved in Lip-1-induced cell death at the transcriptome level.

ER stress and autophagy are involved in Lip-1 induced K562 cells. To identify whether the expanded ER was related to ER stress, the expression levels of CHOP and PUMA, both of which are associated with ER stress-mediated apoptosis, were examined (34). As expected, transcriptome and protein levels of CHOP and PUMA were elevated in Lip-1-treated K562 cells (Fig. 4A and B). To explore whether Lip-1 induced autophagy in K562 cells, RT-qPCR and western blotting were performed; it was determined that LC3B gene expression was significantly increased in Lip-1-treated cells than in untreated cells and the expression of LC3B-II, a hallmark product of autophagy, was markedly increased after 24-h treatment of K562 cells with

10 or 20 μM Lip-1 (Fig. 4A and B). To visualize the formation of autophagosomes, immunofluorescence staining was performed; using a confocal laser scanning microscope, it was observed that the number of LC3 puncta was increased in Lip-1-treated cells (Fig. 4C). These results collectively indicated that treatment with Lip-1 potently induced ER stress and autophagy in K562 cells.

Lip-1 induces p21$^{WAF1/CIP1}$-mediated cell cycle arrest in K562 cells. To investigate the inhibitory effect of cell proliferation, flow cytometry was performed to analyze the cell-cycle distribution. As revealed in Fig. 5A, the proportion of cells in the S phase decreased in a concentration-dependent manner, but the opposite changes were noted in the proportion of cells in the G2/M phase upon treatment with 10 or 20 μM Lip-1 for 24 h.
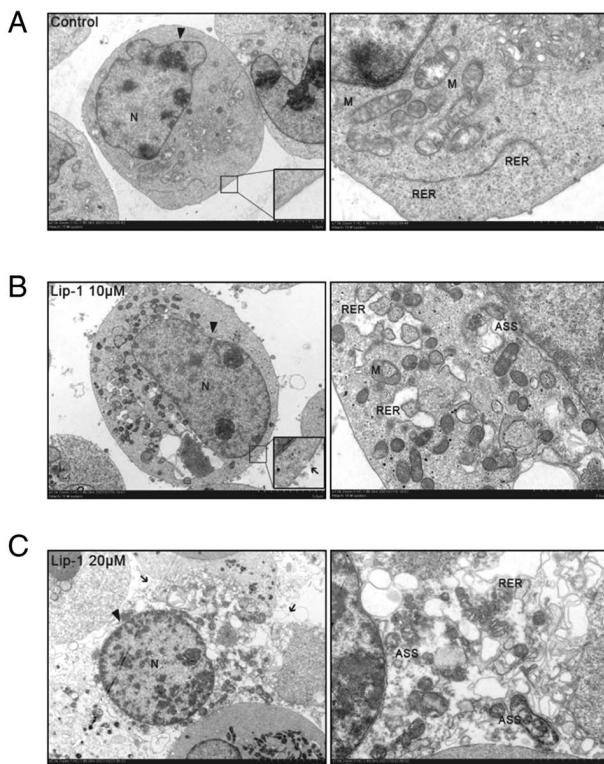
Figure 2. Representative transmission electron micrographs of K562 cells treated with Lip-1. (A) Untreated K562 cells characterized by unexpanded RER with the plasma membrane intact. (B) Expanded RER, ruptured plasma membrane, and ASS observed in K562 cells treated with 10 μM Lip-1 for 24 h. (C) Post-treatment with 20 μM Lip-1 for 24 h. K562 cells were characterized by swelling, ruptured plasma membrane, expanded RER, and an abundance of ASS. N, nuclear; M, mitochondrion. Arrowheads indicate the nuclear membrane; arrows indicate the ruptured plasma membrane. Scale bars, 5 and 2 μm for x2,500 and x7,000 images, respectively. Lip-1, liproxstatin-1; RER, rough endoplasmic reticulum; ASS, autolysosomes.

Flow cytometric results indicated that Lip-1 arrested the cell cycle at the G1 phase in both experimental groups, but cell cycle at the G2 or M phase was only observed in the group treated with a higher concentration of Lip-1. p21$^{WAF1/CIP1}$, a universal inhibitor of cyclin-dependent kinases (35,36), was upregulated in K562 cells treated with Lip-1 compared with that in untreated cells at the transcriptome level (Fig. 5B). Western blot analysis demonstrated that p21$^{WAF1/CIP}$ was highly expressed in Lip-1-treated K562 cells but expressed at a very low level in normal K562 cells (Fig. 5C). Taken together, the data indicated that Lip-1 markedly upregulated p21$^{WAF1/CIP}$ expression and induced cell cycle arrest.

Lip-1 induces apoptosis, caspase-3/GSDME-dependent secondary pyroptosis, and DNA damage in K562 cells. To investigate the function of the plasma membrane, an Annexin V-FITC/PI double staining assay was performed. Because PI cannot penetrate an unimpaired plasma membrane, the increase in the PI-positive cell population indicated that Lip-1 damaged the plasma membrane (Fig. 6A). TNF-α can activate the extrinsic apoptotic signaling pathway as a type of death ligand (37). Thus, it was determined that the gene expression of TNF-α was significantly increased in Lip-1-treated cells compared to that in untreated cells (Fig. 6B). Subsequently, ELISA was used to assess TNF-α protein levels in cell

supernatants and lysates. Limited by the sensitivity of the ELISA kit used, the TNF-α concentration was undetectable in the cell supernatant in the control group and in the lower concentration experimental group (Lip-1 10 μM); however, the TNF-α concentration in another experimental group (Lip-1, 20 μM) was 10.2 pg/ml on average (Fig. 6C, left panel). The concentration of TNF-α in cell lysates was greater in the higher concentration experimental group (Lip-1, 20 μM) than in the control group; the same was true for supernatants (Fig. 6C, right panel). It was also found that the protein level of BAX was upregulated in Lip-1-treated K562 cells (Fig. 6D), indicating that the intrinsic apoptotic signaling pathway was involved in Lip-1-induced cell death.

Caspase-3 is an executor in both intrinsic and extrinsic apoptosis, and it can be cleaved into different subunits to execute biological functions (10,38,39). Western blot analysis revealed that caspase-3 was activated in Lip-1-treated cells in a dose-dependent manner (Fig. 6D). Accompanied by caspase-3 activation, PARP, as a substrate of caspase-3 (40), was cleaved into an 89-kDa fragment (Fig. 6D). The colorimetric assay was performed to validate and quantify the activation of caspase-3 (Fig. 6E, left panel). Although caspase-3 is a hallmark of apoptosis, in this scenario, the morphology and appearance of the dying cells treated with 20 μM Lip-1 were not consistent with typical apoptotic cells. Furthermore, caspase-1 was not activated in Lip-1-treated K562 cells (Fig. 6E, right panel). Some dying cells were rescued upon using the caspase-3-specific inhibitor z-DEVD-FMK, and the protein level of N-terminal GSDME was reduced after z-DEVD-FMK treatment (Fig. 6F). RT-qPCR results demonstrated that the gene expression of GSDME was upregulated in both experimental groups compared to that in the control group (Fig. 6G). However, the protein level of the cleaved N-terminal GSDME, which plays a key role in cell pyroptosis, only increased in K562 cells treated with 20 μM Lip-1 for 24 h (Fig. 6H). In addition, it was determined that K562 cells expressed little GSDME compared to positive control SH-SY5Y cells, based on the integrated density of the loading control (Fig. 6H). These results indicated that Lip-1 treatment potently induced cell apoptosis and secondary pyroptosis and that the induction of secondary pyroptosis in K562 cells was caspase-3/GSDME-dependent and not caspase-1/GSDMD-dependent.

Finally, the terminal deoxynucleotidyl transferase dUTP nick-end labelling (TUNEL) assay was performed to evaluate DNA fragmentation. It was determined that the number of TUNEL-positive cells increased in a concentration-dependent manner (Fig. 6I). Therefore, Lip-1 is considered to be a type of DNA-damaging drug.

Discussion

Lip-1, a spiroquinoxalinamine derivative, was first discovered in a library of small molecules in 2014 (25), and has since been used as a ferroptosis inhibitor. Lip-1 physically disrupts the outer membrane of gram-negative bacteria (26). However, the anticancer effects of Lip-1 have not yet been reported. In the present study, it was determined that Lip-1 inhibits K562 leukemia cell proliferation by inducing cell cycle arrest, apoptosis, and secondary pyroptosis, and it is considered that the
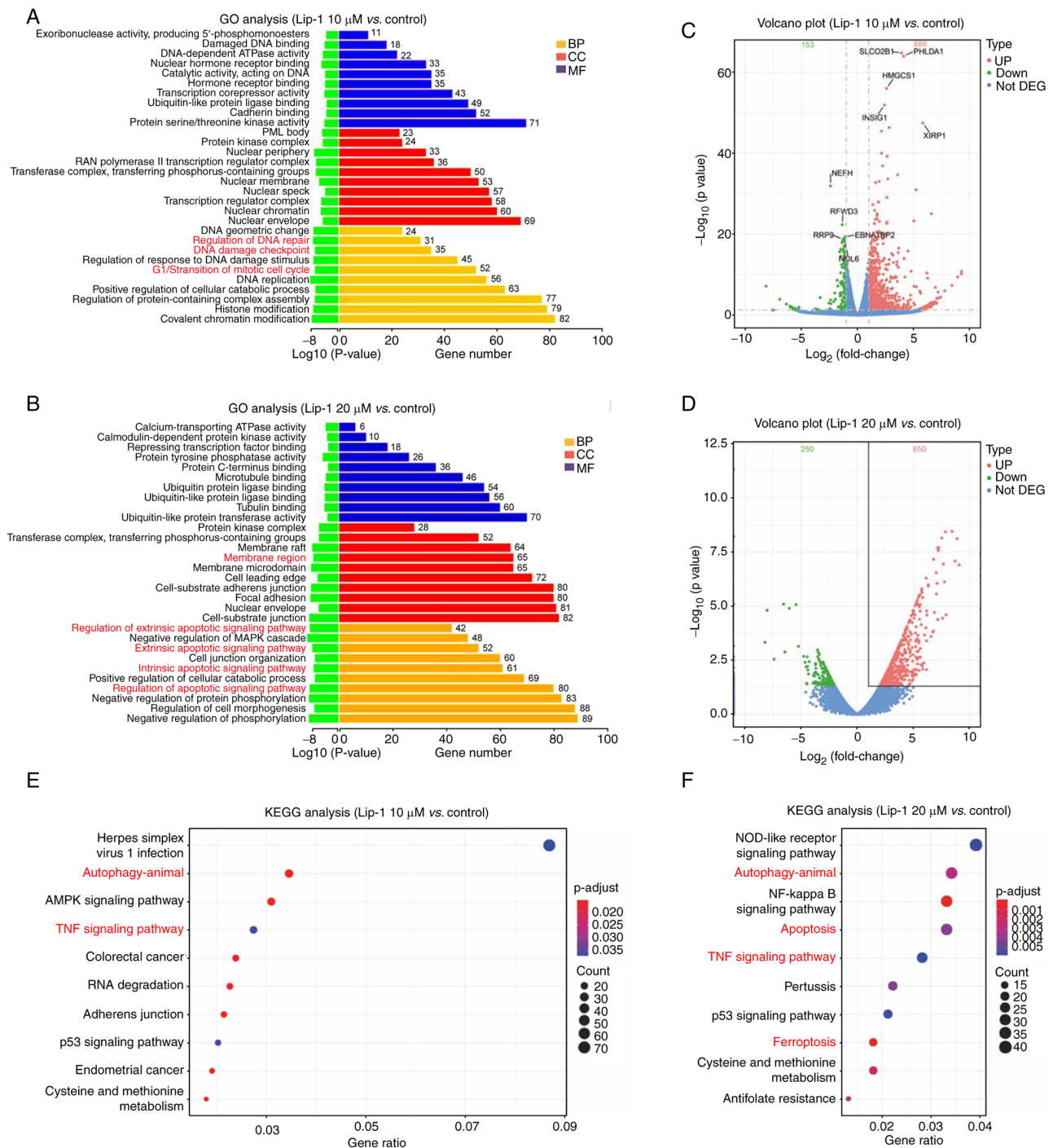
Figure 3. RNA sequencing analysis of the effect of Lip-1 on the expression profile of K562 cells. (A and B) Gene Ontology annotations of DEGs were summarized according to biological process, cellular component, and molecular function. (C and D) Volcano plots were used to visualize DEGs between the Lip-1-treated and control groups. (E and F) Top 10 enriched Kyoto Encyclopedia of Genes and Genomes pathways in 10 and 20 μM Lip-1-treated K562 cells compared to the control group. p.adjust, Benjamini-Hochberg adjusted P-value. Lip-1, liproxstatin-1; GO, Gene Ontology; DEGs, differentially expressed genes; BP, biological process; CC, cellular component; MF, molecular function; KEGG, Kyoto Encyclopedia of Genes and Genomes.

apoptosis-to-pyroptosis switch requires relatively high levels of GSDME and caspase-3 activation.

GSDME belongs to the gasdermin family, and cleavage of GSDME by caspase-3 during apoptosis mediates progression to secondary pyroptosis (16). Caspase-3 plays a key role in apoptosis and can be induced via extrinsic or intrinsic apoptotic signaling pathways. Extrinsic apoptosis is initiated by death receptors, including TNFR1/2 and TRAILR1/2. Once ligand binding occurs, such as TNF-α binding to TNFR1,

the adaptor protein Fas-associated death domain protein is recruited, followed by initiator caspase (caspase-8/-10) and downstream executioner caspase activation (mainly caspase-3/-7) (10,41). Intrinsic apoptosis is initiated by a variety of microenvironmental perturbations, such as DNA damage, ER stress, and mitotic defects (10). Subsequently, mitochondrial outer membrane permeabilization results in the release of cytochrome c, which activates caspase-9 (an initiator caspase) and downstream caspase-3 (an executioner
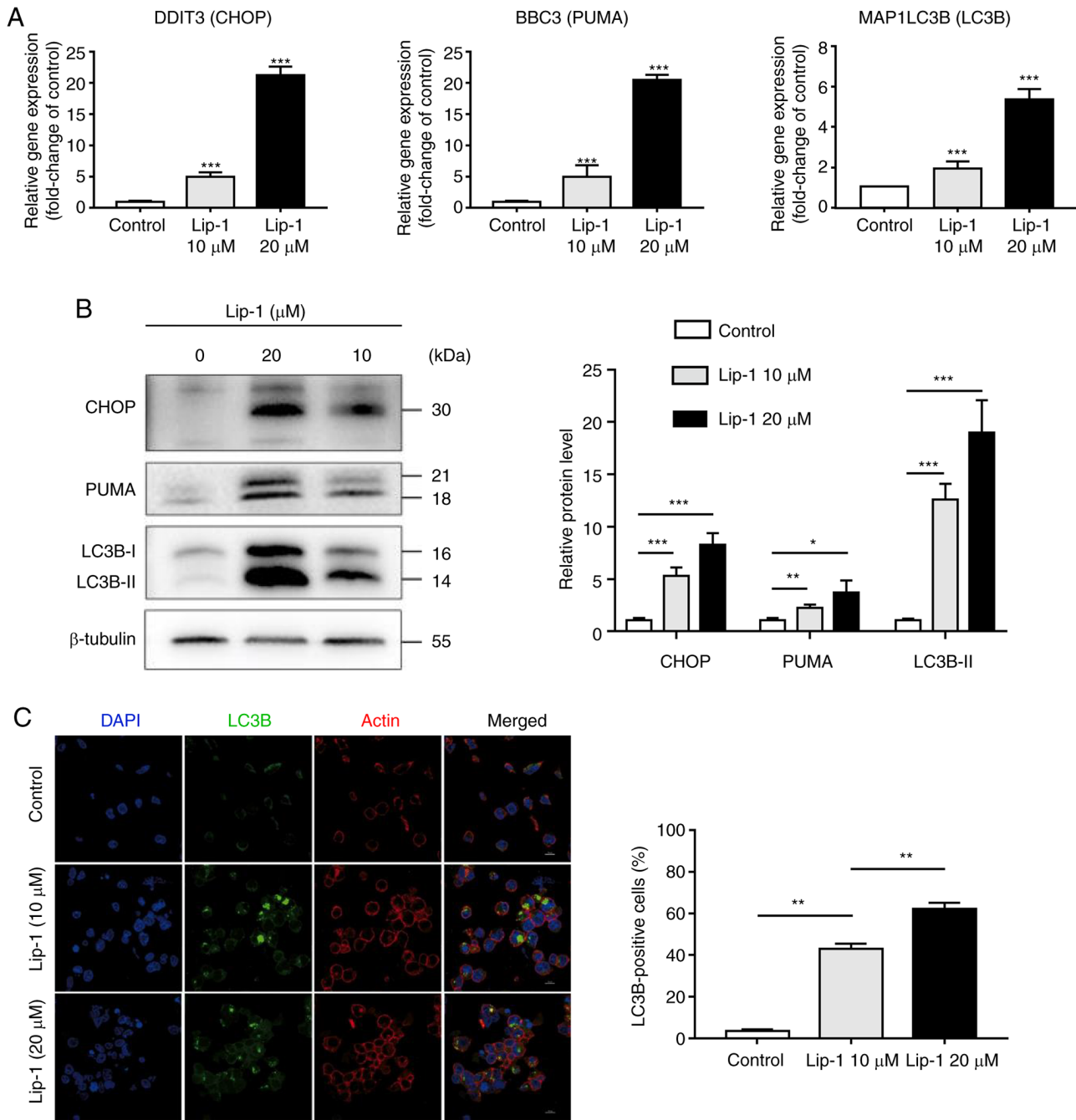
Figure 4. Endoplasmic reticulum stress and autophagy in Lip-1-induced K562 cells. K562 cells were treated with 10 and 20 μM Lip-1 for 24 h. (A) The expression levels of CHOP, PUMA, and LC3B measured by real-time polymerase chain reaction and normalized to RPLP0. (B) CHOP, PUMA, and LC3B protein levels quantified by western blotting and normalized to β-tubulin. (C) Immunofluorescence staining of LC3B and actin in K562 cells. Nuclei were counterstained with DAPI. Scale bar, 10 μm. Data represent the mean ± SD from three independent experiments. *P<0.05, **P<0.01 and ***P<0.001 vs. Control. Lip-1, liproxstatin-1; CHOP, C/EBP homologous.

caspase) (20,41,42). Proapoptotic (BAX/BIM/PUMA) and antiapoptotic (BCL2/BCL-X$_L$/BCL-W) members of the BCL2 family are involved in the release of cytochrome *c* (10). Of note, ER stress is a common cellular process that responds to microenvironmental perturbations. If ER-stressed cells cannot restore their capacity for protein folding, they commit to self-destruction via the induction of CHOP, which inhibits the expression of BCL2 and upregulates BIM (43). Herein, it was determined that both extrinsic and intrinsic apoptotic signaling pathways are involved in Lip-1-induced cell death via RNA-seq. The expression of BAX and TNF-α, which

represent intrinsic and extrinsic apoptosis, respectively, were further investigated. BAX was upregulated in both experimental groups, whereas TNF-α overexpression was observed only in the experimental group treated with higher concentrations of Lip-1. Using several techniques, it was determined that caspase-3 was activated in a dose- and time-dependent manner. However, apoptotic cells did not exhibit a typical apoptotic appearance. By contrast, cell swelling, membrane rupture, and ER expansion was observed in Lip-1-treated K562 cells. The plasma membrane remains intact in apoptotic cells until the very late stage of apoptosis, and apoptotic cells
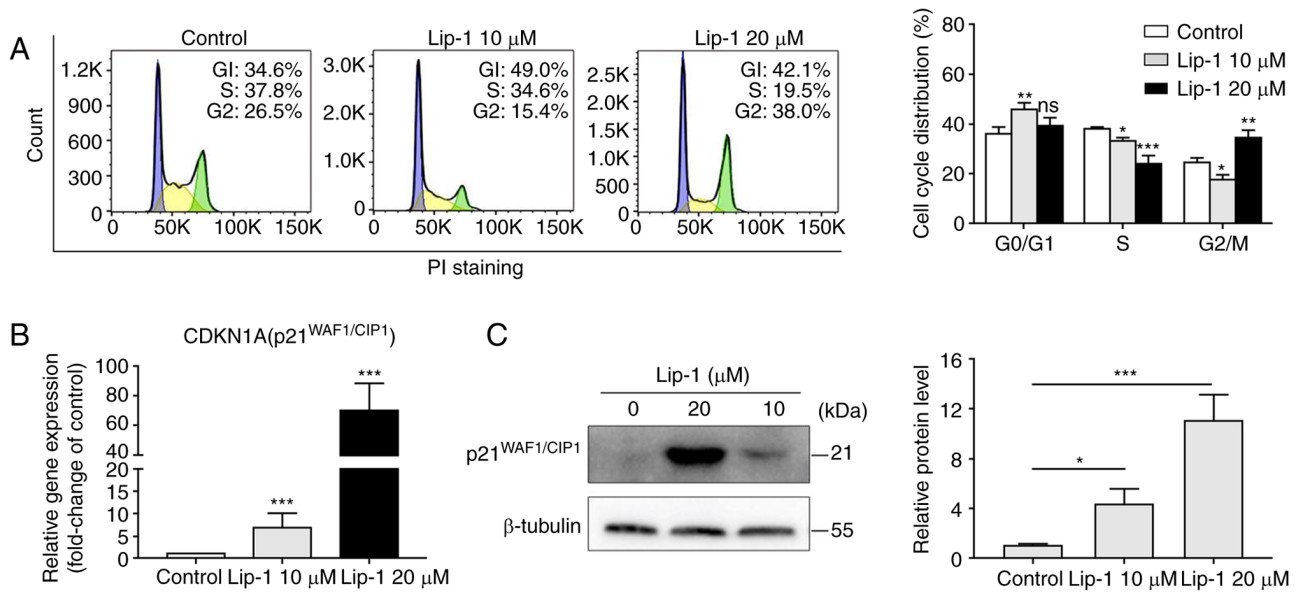
Figure 5. Lip-1 induces cell cycle arrest through p21[WAF1/CIP1] upregulation in K562 cells. K562 cells were treated with 10 and 20 μM Lip-1 for 24 h. (A) Cell cycle phase distribution of K562 cells determined by flow cytometry. (B) Expression level of CDKN1A (p21[WAF1/CIP1]) assessed by real-time polymerase chain reaction and normalized to RPLP0. (C) p21[WAF1/CIP1] protein level quantified by western blotting and normalized to β-tubulin. Data represent the mean ± SD from three independent experiments. [*]P<0.05, [**]P<0.01 and [***]P<0.001 vs. Control. Lip-1, liproxstatin-1; ns, not significant.

are characterized by cell shrinkage, not swelling (44). The morphology of Lip-1-treated K562 cells was very different from that of apoptotic cells; therefore, it was hypothesized that necrosis or pyroptosis may occur in Lip-1-induced cell death. Cleaved N-terminal GSDME production was then assessed and it was observed that Lip-1-induced apoptosis mediated progression to secondary pyroptosis. Additionally, the expanded ER and increased expression of CHOP and PUMA suggested that ER stress plays a role in Lip-1-induced cell death. In the past few decades, researchers have designed numerous drugs targeting the apoptotic pathway, including BH3 mimetics, stapled peptides, and IAP inhibitors, some of which have achieved favorable clinical results (41). The use of venetoclax (a novel selective BCL2 inhibitor) is successful; however, the possibility of primary or acquired drug resistance should not be ignored (45,46). Pyroptosis has several advantages over apoptosis, such as induction of faster cell death and activation of antitumor immunity (16,19), indicating that targeting the pyroptosis pathway is a better therapeutic strategy than targeting the apoptotic pathway. Therefore, theoretically, venetoclax-resistant cells could respond to Lip-1 (a pyroptosis inducer).

Various types of RCD occur in distinct cells treated concurrently with a specific drug *in vitro*. End-stage apoptosis is usually followed by rupture of the plasma membrane and the development of a necrotic morphotype (secondary necrosis) (10,47). Guzik *et al* (48) elucidated that neutrophil exposure to cigarette smoke extract leads to atypical cell death with features shared among autophagy, apoptosis, and necrosis. In another study (49), necrotic cells were often observed concurrently with apoptotic cells, when the cells were treated with parthenolide at the same concentration. In the present study, both apoptotic and pyroptotic cells were observed. Consistent with the results from earlier studies (13,16), cells with high levels of GSDME developed secondary pyroptosis

following apoptosis. Therefore, it is considered that the dying cells were undergoing apoptosis and that apoptosis and pyroptosis in Lip-1-treated K562 cells occurred sequentially.

Different types of RCD occasionally share the same upstream molecules; accordingly, crosstalk between RCD pathways is inevitable. Ferroptosis is an iron-dependent form of RCD, and differs from apoptosis by excessive lipid peroxidation, lack of glutathione, and inactivation of caspase-3 (50,51). However, a recent study demonstrated that the ER stress-mediated CHOP-PUMA pathway was associated with the interaction between apoptosis and ferroptosis (52). Moreover, p53 is a key factor that mediates the crosstalk between apoptosis and ferroptosis (53-55). Caspase-3 plays a central role in both apoptosis and pyroptosis, and whether cells undergo pyroptosis depends on the expression of GSDME, a downstream molecule of caspase-3 (13). A recent study by Rogers *et al* (56) demonstrated that cleaved N-terminal GSDME targets the mitochondria to release cytochrome *c* and activate caspase-3. The interaction between apoptosis and pyroptosis is delicate and complex. TNF-α acts as a death ligand in the extrinsic apoptotic pathway and initiates caspase-8 activation (10). TNF-α is also a crucial signaling molecule in the necroptotic pathway; however, in necroptosis, the activity of caspase-8 is suppressed, which eventually results in the expression of RIPK1/3, exerting a series of autophosphorylation or transphosphorylation effects (10,57,58). In the present study, it was determined that TNF-α and activated caspase-3 were highly expressed in Lip-1-treated K562 cells, and that the caspase-3-specific inhibitor z-DEVD-FMK could not completely reverse cell death. Therefore, it was hypothesized that another type of RCD may be involved in Lip-1-induced cell death. Cell cycle progression and division are regulated by cyclins, cyclin-dependent kinases, and cyclin-dependent kinase inhibitors. There are three main checkpoints: G1, G2/M, and metaphase (59). Non-functional checkpoints result
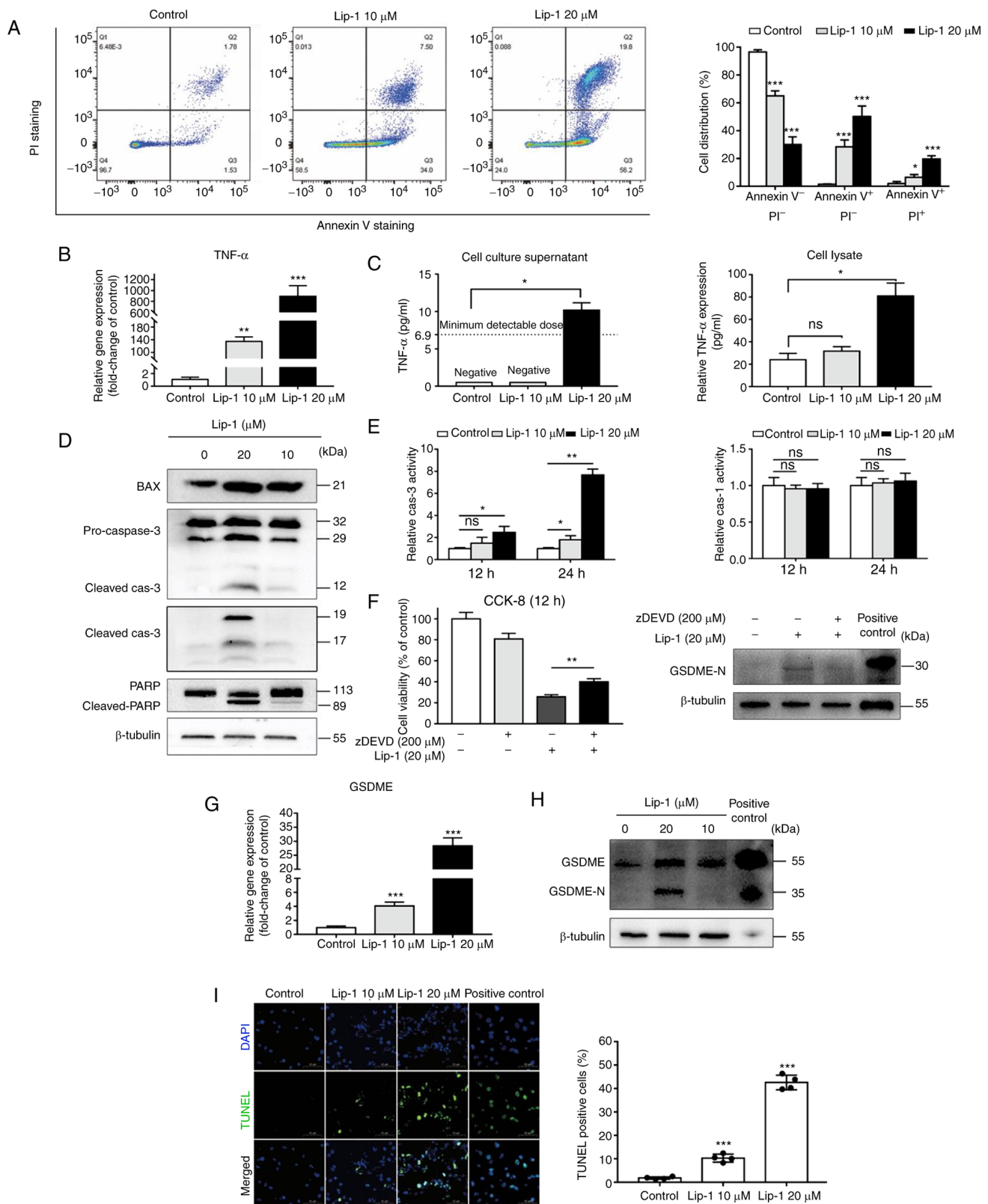
Figure 6. Lip-1 induces pyroptosis in K562 leukemia cells via caspase-3/GSDME activation. K562 cells were treated with 10 and 20 μM Lip-1 for 24 h in most experiments; part F shows an experiment in which K562 cells were pretreated with z-DEVD-FMK for 3 h and further treated with 20 μM Lip-1 for 12 h. (A) K562 cells double-stained with Annexin V-FITC/PI for flow cytometry. (B) Expression levels of TNF-α assessed by real-time polymerase chain reaction and normalized to RPLP0. (C) Protein levels of TNF-α in cell culture supernatants and cell lysates detected by enzyme-linked immunosorbent assay (minimum detectable concentration, 6.9 pg/ml). (D) BAX, cleaved caspase-3, and cleaved PARP protein levels quantified by western blotting. (E) Lip-1 induced caspase-3, but not caspase-1, activation in a concentration- and time-dependent manner. Caspase-1/-3 activities were measured by colorimetric assay. (F) Comparison of cell viability and the protein level of N-terminal GSDME in Lip-1-treated K562 cells and the effects of z-DEVD-FMK inhibition. SH-SY5Y whole cell lysate was used as a positive control. (G) Expression levels of GSDME assessed by real-time polymerase chain reaction and normalized to RPLP0. (H) GSDME and cleaved N-terminal GSDME protein levels quantified by western blotting. SH-SY5Y whole cell lysate was used as a positive control. (I) TUNEL assay used to determine DNA fragmentation. Specimens treated with DNase I were used as positive controls. Data represent the mean ± SD from at least three independent experiments. *P<0.05, **P<0.01 and ***P<0.001 vs. Control. Lip-1, liproxstatin-1; ns, not significant.

in uncontrolled cell proliferation (60), and unscheduled cell division is a hallmark of malignant tumors. In the past few decades, scientists have developed adequate cell cycle therapeutics. Palbociclib, a CDK4/6 inhibitor, has been used to treat breast cancer (61). Cytarabine, a first-line drug for the treatment of leukemia, kills leukemic cells by blocking the cell cycle at the G1 phase (6). In the present study, it was determined that the G1/S transition of the mitotic cell cycle was associated with Lip-1-induced cell death via RNA-seq. Flow cytometry revealed that Lip-1 arrested the cell cycle at the G1 phase, and even at the G2/M phase. Moreover, p21$^{WAF1/CIP1}$, a member of the CIP/KIP family, was upregulated in Lip-1-treated K562 cells. As a type of cyclin-dependent kinase inhibitor, p21$^{WAF1/CIP1}$ can block the cell cycle at different phases by inhibiting numerous types of cyclin/cyclin-dependent kinase complexes, including cyclin A/E-CDK2, cyclin A-CDK1, and cyclin B-CDK1 (61,62). Thus, Lip-1 is a potential cell cycle therapeutic agent.

There are some limitations to the present study. First, numerous cancers express low levels of GSDME owing to aberrant promoter hypermethylation, and demethylation treatment increases cellular susceptibility to apoptosis (63-65). In a previous study, it was revealed that the expression of GSDME in K562 cells is very low, and cells develop secondary necrosis after apoptosis when lacking sufficient GSDME (13). Upon treatment with Lip-1, GSDME expression increased, and it is considered that K562 cells underwent secondary pyroptosis, not necrosis, after apoptosis. Thus, whether Lip-1 has demethylation effects requires further investigation. Second, although autophagy is considered a survival process to maintain cellular homeostasis, autophagy-dependent cell death is a novel type of RCD (10,21). It was determined that autophagy is involved in Lip-1-induced cell death; however, whether it is beneficial or harmful to cell survival remains unknown. Third, p21$^{WAF1/CIP1}$ was upregulated in K562 cells; however, how p21$^{WAF1/CIP1}$ delicately modulated the cell cycle remains unclear. Thus, p21 knockdown or knockout should be performed in future studies. Finally, GSDME is highly expressed in various normal tissues (63,66), and high levels of GSDME increase the side effects of chemotherapeutic drugs (13,19). The efficacy and side effects of Lip-1 treatment *in vivo* were not determined; therefore, it is difficult to elucidate the role of Lip-1 in leukemogenesis. The underlying mechanisms should be studied further.

In conclusion, it was revealed that Lip-1 inhibits K562 cell proliferation *in vitro*. To the best of our knowledge, the present study is the first to report that Lip-1 treatment induces cell cycle arrest, apoptosis, and caspase-3/GSDME-dependent secondary pyroptosis in K562 leukemia cells. Moreover, caspase-3 activation and relatively high levels of GSDME were revealed to be responsible for inducing secondary pyroptosis. Additionally, ER stress and autophagy were involved in Lip-1-induced cell death. These findings provide new insights into Lip-1 as a promising candidate for the treatment of leukemia. This research would be the base for further studies.

Availability of data and materials

The data generated in the present study may be requested from the corresponding author.

Authors' contributions

HQD contributed to the design of the study. HQD, SJL, PC, YLX, YD, NS, and DHD contributed to the acquisition, analysis, or interpretation of the data. HQD and SJL drafted the manuscript, and PC revised it critically for important intellectual content. HQD and PC confirm the authenticity of all the raw data. All authors read and approved the final version to be published and agree to be accountable for all aspects of the work in ensuring that questions related to the accuracy or integrity of any part of the work are appropriately investigated and resolved.

Ethics approval and consent to participate

Not applicable.

Patient consent for publication

Not applicable.

Competing interests

The authors declare that they have no competing interests.

References

1. Bonnet D and Dick JE: Human acute myeloid leukemia is organized as a hierarchy that originates from a primitive hematopoietic cell. Nat Med 3: 730-737, 1997.
2. Steinwascher S, Nugues AL, Schoeneberger H and Fulda S: Identification of a novel synergistic induction of cell death by Smac mimetic and HDAC inhibitors in acute myeloid leukemia cells. Cancer Lett 366: 32-43, 2015.
3. Tamm I, Kornblau SM, Segall H, Krajewski S, Welsh K, Kitada S, Scudiero DA, Tudor G, Qui YH, Monks A, *et al*: Expression and prognostic significance of IAP-family genes in human cancers and myeloid leukemias. Clin Cancer Res 6: 1796-1803, 2000.
4. Zeng H, Chen W, Zheng R, Zhang S, Ji JS, Zou X, Xia C, Sun K, Yang Z, Li H, *et al*: Changing cancer survival in China during 2003-15: A pooled analysis of 17 population-based cancer registries. Lancet Glob Health 6: e555-e567, 2018.
5. Long L, Assaraf YG, Lei ZN, Peng H, Yang L, Chen ZS and Ren S: Genetic biomarkers of drug resistance: A compass of prognosis and targeted therapy in acute myeloid leukemia. Drug Resist Updat 52: 100703, 2020.

6. Murphy T and Yee KWL: Cytarabine and daunorubicin for the treatment of acute myeloid leukemia. Expert Opin Pharmacother 18: 1765-1780, 2017.
7. DiNardo CD, Pratz K, Pullarkat V, Jonas BA, Arellano M, Becker PS, Frankfurt O, Konopleva M, Wei AH, Kantarjian HM, *et al*: Venetoclax combined with decitabine or azacitidine in treatment-naive, elderly patients with acute myeloid leukemia. Blood 133: 7-17, 2019.
8. Carter JL, Hege K, Yang J, Kalpage HA, Su Y, Edwards H, Hüttemann M, Taub JW and Ge Y: Targeting multiple signaling pathways: The new approach to acute myeloid leukemia therapy. Signal Transduct Target Ther 5: 288, 2020.
9. Xia X, Wang X, Cheng Z, Qin W, Lei L, Jiang J and Hu J: The role of pyroptosis in cancer: Pro-cancer or pro-'host'? Cell Death Dis 10: 650, 2019.
10. Galluzzi L, Vitale I, Aaronson SA, Abrams JM, Adam D, Agostinis P, Alnemri ES, Altucci L, Amelio I, Andrews DW, *et al*: Molecular mechanisms of cell death: Recommendations of the Nomenclature Committee on Cell Death 2018. Cell Death Differ 25: 486-541, 2018.
11. Ding J, Wang K, Liu W, She Y, Sun Q, Shi J, Sun H, Wang DC and Shao F: Pore-forming activity and structural autoinhibition of the gasdermin family. Nature 535: 111-116, 2016.
12. Kuang S, Zheng J, Yang H, Li S, Duan S, Shen Y, Ji C, Gan J, Xu XW and Li J: Structure insight of GSDMD reveals the basis of GSDMD autoinhibition in cell pyroptosis. Proc Natl Acad Sci USA 114: 10642-10647, 2017.
13. Wang Y, Gao W, Shi X, Ding J, Liu W, He H, Wang K and Shao F: Chemotherapy drugs induce pyroptosis through caspase-3 cleavage of a gasdermin. Nature 547: 99-103, 2017.
14. Shi J, Zhao Y, Wang K, Shi X, Wang Y, Huang H, Zhuang Y, Cai T, Wang F and Shao F: Cleavage of GSDMD by inflammatory caspases determines pyroptotic cell death. Nature 526: 660-665, 2015.
15. Wang YY, Liu XL and Zhao R: Induction of pyroptosis and its implications in cancer management. Front Oncol 9: 971, 2019.
16. Rogers C, Fernandes-Alnemri T, Mayes L, Alnemri D, Cingolani G and Alnemri ES: Cleavage of DFNA5 by caspase-3 during apoptosis mediates progression to secondary necrotic/pyroptotic cell death. Nat Commun 8: 14128, 2017.
17. Johnson DC, Taabazuing CY, Okondo MC, Chui AJ, Rao SD, Brown FC, Reed C, Peguero E, de Stanchina E, Kentsis A and Bachovchin DA: DPP8/DPP9 inhibitor-induced pyroptosis for treatment of acute myeloid leukemia. Nat Med 24: 1151-1156, 2018.
18. Yang W, Liu S, Li Y, Wang Y, Deng Y, Sun W, Huang H, Xie J, He A, Chen H, *et al*: Pyridoxine induces monocyte-macrophages death as specific treatment of acute myeloid leukemia. Cancer Lett 492: 96-105, 2020.
19. Zhang Z, Zhang Y and Lieberman J: Lighting a fire: Can we harness pyroptosis to ignite antitumor immunity? Cancer Immunol Res 9: 2-7, 2021.
20. Jiang M, Qi L, Li L and Li Y: The caspase-3/GSDME signal pathway as a switch between apoptosis and pyroptosis in cancer. Cell Death Discov 6: 112, 2020.
21. Klionsky DJ, Petroni G, Amaravadi RK, Baehrecke EH, Ballabio A, Boya P, Bravo-San Pedro JM, Cadwell K, Cecconi F, Choi AMK, *et al*: Autophagy in major human diseases. EMBO J 40: e108863, 2021.
22. Tang R, Xu J, Zhang B, Liu J, Liang C, Hua J, Meng Q, Yu X and Shi S: Ferroptosis, necroptosis, and pyroptosis in anticancer immunity. J Hematol Oncol 13: 110, 2020.
23. Galluzzi L and Green DR: Autophagy-independent functions of the autophagy machinery. Cell 177: 1682-1699, 2019.
24. Frank D and Vince JE: Pyroptosis versus necroptosis: Similarities, differences, and crosstalk. Cell Death Differ 26: 99-114, 2019.
25. Friedmann Angeli JP, Schneider M, Proneth B, Tyurina YY, Tyurin VA, Hammond VJ, Herbach N, Aichler M, Walch A, Eggenhofer E, *et al*: Inactivation of the ferroptosis regulator Gpx4 triggers acute renal failure in mice. Nat Cell Biol 16: 1180-1191, 2014.
26. Klobucar K, Côté JP, French S, Borrillo L, Guo ABY, Serrano-Wu MH, Lee KK, Hubbard B, Johnson JW, Gaulin JL, *et al*: Chemical screen for vancomycin antagonism uncovers probes of the gram-negative outer membrane. ACS Chem Biol 16: 929-942, 2021.
27. Lozzio CB and Lozzio BB: Human chronic myelogenous leukemia cell-line with positive Philadelphia chromosome. Blood 45: 321-334, 1975.
28. Pertea M, Pertea GM, Antonescu CM, Chang TC, Mendell JT and Salzberg SL: StringTie enables improved reconstruction of a transcriptome from RNA-seq reads. Nat Biotechnol 33: 290-295, 2015.
29. Love MI, Huber W and Anders S: Moderated estimation of fold change and dispersion for RNA-seq data with DESeq2. Genome Biol 15: 550, 2014.
30. Gene Ontology Consortium: Gene ontology consortium: Going forward. Nucleic Acids Res 43(Database Issue): D1049-D1056, 2015.
31. Kanehisa M, Araki M, Goto S, Hattori M, Hirakawa M, Itoh M, Katayama T, Kawashima S, Okuda S, Tokimatsu T and Yamanishi Y: KEGG for linking genomes to life and the environment. Nucleic Acids Res 36(Database Issue): D480-D484, 2008.
32. Yu G, Wang LG, Han Y and He QY: clusterProfiler: An R package for comparing biological themes among gene clusters. OMICS 16: 284-287, 2012.
33. Livak KJ and Schmittgen TD: Analysis of relative gene expression data using real-time quantitative PCR and the 2(-Delta Delta C(T)) method. Methods 25: 402-408, 2001.
34. Zhao X, Zhu L, Liu D, Chi T, Ji X, Liu P, Yang X, Tian X and Zou L: Sigma-1 receptor protects against endoplasmic reticulum stress-mediated apoptosis in mice with cerebral ischemia/reperfusion injury. Apoptosis 24: 157-167, 2019.
35. Xiong Y, Hannon GJ, Zhang H, Casso D, Kobayashi R and Beach D: p21 is a universal inhibitor of cyclin kinases. Nature 366: 701-704, 1993.
36. Lai L, Shin GY and Qiu H: The role of cell cycle regulators in cell survival-dual functions of cyclin-dependent kinase 20 and p21$^{Cip1/Waf1}$. Int J Mol Sci 21: 8504, 2020.
37. Pistritto G, Trisciuoglio D, Ceci C, Garufi A and D'Orazi G: Apoptosis as anticancer mechanism: Function and dysfunction of its modulators and targeted therapeutic strategies. Aging (Albany NY) 8: 603-619, 2016.
38. Nicholson DW, Ali A, Thornberry NA, Vaillancourt JP, Ding CK, Gallant M, Gareau Y, Griffin PR, Labelle M and Lazebnik YA, *et al*: Identification and inhibition of the ICE/CED-3 protease necessary for mammalian apoptosis. Nature 376: 37-43, 1995.
39. Kavanagh E, Rodhe J, Burguillos MA, Venero JL and Joseph B: Regulation of caspase-3 processing by cIAP2 controls the switch between pro-inflammatory activation and cell death in microglia. Cell Death Dis 5: e1565, 2014.
40. Cohen GM: Caspases: The executioners of apoptosis. Biochem J 326 (Pt 1): 1-16, 1997.
41. Carneiro BA and El-Deiry WS: Targeting apoptosis in cancer therapy. Nat Rev Clin Oncol 17: 395-417, 2020.
42. Nikoletopoulou V, Markaki M, Palikaras K and Tavernarakis N: Crosstalk between apoptosis, necrosis and autophagy. Biochim Biophys Acta 1833: 3448-3459, 2013.
43. Oakes SA and Papa FR: The role of endoplasmic reticulum stress in human pathology. Annu Rev Pathol 10: 173-194, 2015.
44. Bortner CD and Cidlowski JA: Ions, the movement of water and the apoptotic volume decrease. Front Cell Dev Biol 8: 611211, 2020.
45. Saliba AN, John AJ, and Kaufmann SH: Resistance to venetoclax and hypomethylating agents in acute myeloid leukemia. Cancer Drug Resist 4: 125-142, 2021.
46. Blombery P: Mechanisms of intrinsic and acquired resistance to venetoclax in B-cell lymphoproliferative disease. Leuk Lymphoma 61: 257-262, 2020.
47. Vanden Berghe T, Vanlangenakker N, Parthoens E, Deckers W, Devos M, Festjens N, Guerin CJ, Brunk UT, Declercq W and Vandenabeele P: Necroptosis, necrosis and secondary necrosis converge on similar cellular disintegration features. Cell Death Differ 17: 922-930, 2010.
48. Guzik K, Skret J, Smagur J, Bzowska M, Gajkowska B, Scott DA, and Potempa JS: Cigarette smoke-exposed neutrophils die unconventionally but are rapidly phagocytosed by macrophages. Cell Death Dis 2: e131, 2011.
49. Pozarowski P, Halicka DH and Darzynkiewicz Z: Cell cycle effects and caspase-dependent and independent death of HL-60 and Jurkat cells treated with the inhibitor of NF-kappaB parthenolide. Cell Cycle 2: 377-383, 2003.
50. Xia H, Zhang Z and You F: Inhibiting ACSL1-related ferroptosis restrains murine coronavirus infection. Viruses 13: 2383, 2021.
51. Lin L, Zhang MX, Zhang L, Zhang D, Li C and Li YL: Autophagy, pyroptosis, and ferroptosis: New regulatory mechanisms for atherosclerosis. Front Cell Dev Biol 9: 809955, 2022.

52. Lee YS, Lee DH, Choudry HA, Bartlett DL and Lee YJ: Ferroptosis-induced endoplasmic reticulum stress: Cross-talk between ferroptosis and apoptosis. Mol Cancer Res 16: 1073-1076, 2018.
53. Chu B, Kon N, Chen D, Li T, Liu T, Jiang L, Song S, Tavana O and Gu W: ALOX12 is required for p53-mediated tumour suppression through a distinct ferroptosis pathway. Nat Cell Biol 21: 579-591, 2019.
54. Jiang L, Kon N, Li T, Wang SJ, Su T, Hibshoosh H, Baer R and Gu W: Ferroptosis as a p53-mediated activity during tumour suppression. Nature 520: 57-62, 2015.
55. Zheng DW, Lei Q, Zhu JY, Fan JX, Li CX, Li C, Xu Z, Cheng SX and Zhang XZ: Switching apoptosis to ferroptosis: Metal-organic network for high-efficiency anticancer therapy. Nano Lett 17: 284-291, 2017.
56. Rogers C, Erkes DA, Nardone A, Aplin AE, Fernandes-Alnemri T and Alnemri ES: Gasdermin pores permeabilize mitochondria to augment caspase-3 activation during apoptosis and inflammasome activation. Nat Commun 10: 1689, 2019.
57. Newton K, Wickliffe KE, Dugger DL, Maltzman A, Roose-Girma M, Dohse M, Kőmüves L, Webster JD and Dixit VM: Cleavage of RIPK1 by caspase-8 is crucial for limiting apoptosis and necroptosis. Nature 574: 428-431, 2019.
58. Li J, McQuade T, Siemer AB, Napetschnig J, Moriwaki K, Hsiao YS, Damko E, Moquin D, Walz T, McDermott A, et al: The RIP1/RIP3 necrosome forms a functional amyloid signaling complex required for programmed necrosis. Cell 150: 339-350, 2012.
59. Icard P, Fournel L, Wu Z, Alifano M and Lincet H: Interconnection between metabolism and cell cycle in cancer. Trends Biochem Sci 44: 490-501, 2019.
60. Asghar U, Witkiewicz AK, Turner NC and Knudsen ES: The history and future of targeting cyclin-dependent kinases in cancer therapy. Nat Rev Drug Discov 14: 130-146, 2015.
61. Ingham M and Schwartz GK: Cell-cycle therapeutics come of age. J Clin Oncol 35: 2949-2959, 2017.
62. Dulić V, Kaufmann WK, Wilson SJ, Tlsty TD, Lees E, Harper JW, Elledge SJ and Reed SI: p53-dependent inhibition of cyclin-dependent kinase activities in human fibroblasts during radiation-induced G1 arrest. Cell 76: 1013-1023, 1994.
63. Akino K, Toyota M, Suzuki H, Imai T, Maruyama R, Kusano M, Nishikawa N, Watanabe Y, Sasaki Y, Abe T, et al: Identification of DFNA5 as a target of epigenetic inactivation in gastric cancer. Cancer Sci 98: 88-95, 2007.
64. Kim MS, Chang X, Yamashita K, Nagpal JK, Baek JH, Wu G, Trink B, Ratovitski EA, Mori M and Sidransky D: Aberrant promoter methylation and tumor suppressive activity of the DFNA5 gene in colorectal carcinoma. Oncogene 27: 3624-3634, 2008.
65. Wang CJ, Tang L, Shen DW, Wang C, Yuan QY, Gao W, Wang YK, Xu RH and Zhang H: The expression and regulation of DFNA5 in human hepatocellular carcinoma DFNA5 in hepatocellular carcinoma. Mol Biol Rep 40: 6525-6531, 2013.
66. Van Laer L, Huizing EH, Verstreken M, van Zuijlen D, Wauters JG, Bossuyt PJ, Van de Heyning P, McGuirt WT, Smith RJ, Willems PJ, et al: Nonsyndromic hearing impairment is associated with a mutation in DFNA5. Nat Genet 20: 194-197, 1998.